Task 3. Catalyst Characterization

The objective of this task is to obtain characterization data of the prepared catalysts using routine and selected techniques.

A. TPR Study of Promoter and Support Effects on the Reducibility of Supported Cobalt Fischer-Tropsch Catalysts

Abstract

TPR and H_2 chemisorption with pulse reoxidation were used to study the reducibility of cobalt Fischer-Tropsch catalysts. Different supports (e.g., Al_2O_3, TiO_2, SiO_2, and ZrO_2 modified SiO_2) and a variety of promoters, including noble metals and metal cations, were screened. Addition of Ru and Pt provided a similar effect by decreasing the reduction temperature of Co_3O_4 and for CoO species where a significant CoO-support interaction was present, while Re mainly catalyzed the reduction of CoO. A slight decrease in cluster size was evidenced in H_2 chemisorption/pulse reoxidation with noble metal promotion for catalysts reduced at the same temperature, indicating that smaller Co oxide species that interacts with the support were reduced with the aid of the promoter. Increasing the cobalt loading, and therefore the average Co cluster size, was found to exhibit improved reducibility, by decreasing interactions with the supports. Addition of metal oxides such as B, La, K, and Zr were found to decrease the cobalt cluster size, and caused reduction to shift to higher temperatures.

1. Introduction

Supported cobalt catalysts are important for the Fischer-Tropsch synthesis of high molecular weight, paraffinic waxes, which can be hydrocracked to produce lubricants and diesel fuels. One important focus in the development of this process is the improvement of the catalyst activity by the addition of promoters. These promoters reduce at a lower temperature than cobalt oxides, and

decrease their reduction, presumably by hydrogen spillover from the promoter surface [1-12]. By shifting the reduction temperature of cobalt to lower temperatures, we desire to find an appropriate loading of promoter in order to maximize the availability of active cobalt surface sites for participation in the reaction, after the catalyst has been activated.

2. Experimental

2.1 Catalyst Preparation

Davisil silica gel 644, Degussa P25 Titania (100-200 mesh), Condea Vista Catapal B (γ-alumina Boehmite , 100-200 mesh) and zirconia modified Davisil 952 silica were used as support materials for precipitation of the cobalt FTS catalysts. The cobalt loading was 15% except for the ZrO_2-SiO_2 supported catalysts which contained 20% Co, and the TiO_2 catalysts, which contained 10% Co. A multi-step incipient wetness impregnation method was used to add cobalt to the supports with a drying procedure at 353K in a rotary evaporator following each impregnation. Catalysts with different loadings of ruthenium, platinum, rhenium, or potassium promoter were prepared. Additional catalysts were prepared by incorporating zirconium and lanthanum to the support. Following cobalt addition, the promoter was added by incipient wetness impregnation. The precursors utilized were ruthenium nitrosylnitrate, potassium carbonate, tetraammineplatinum (II) nitrate, rhenium oxide, zirconium nitrate, and lanthanum nitrate, respectively. After promoter addition, the catalysts were then dried in a rotary evaporator at 353K again and calcined at 673K for 4hrs.

BET measurements were conducted using a Micromeritics Tri-Star system for all catalysts were conducted to determine the loss of surface area following loading of the metal. Prior to testing, samples were slowly ramped to 160EC and evacuated for 4hrs to approximately 50mTorr. Results of physisorption are shown below in Table 1.

2.2 Temperature Programmed Reduction (TPR)

Temperature programmed reduction (TPR) profiles of fresh and spent catalysts were recorded using a Zeton Altamira AMI-200 unit. Calcined fresh samples were first purged in flowing inert gas to remove traces of water. TPR was performed using a 10%H_2/Ar mixture referenced to Ar. Resulting profiles were normalized to the height of the main peak such that shifts in the peak positions could be determined.

2.3 H_2 Chemisorption by TPD and % Reducibility by Pulse Reoxidation

The amount of chemisorbed hydrogen was measured using the Zeton Altamira AMI-200 unit, which incorporates a thermal conductivity detector (TCD). The sample weight used was always 0.220 g. A typical catalyst was activated using pure hydrogen at the desired reduction temperature (usually 300 or 350^{o}C) for 10hrs and cooled under flowing hydrogen to 100^{o}C. The sample was held at 100^{o}C under flowing argon to prevent adsorption of physisorbed and weakly bound species, prior to increasing the temperature slowly to the activation temperature. At that temperature, the catalyst was held under flowing argon to desorb the remaining chemisorbed hydrogen until the TCD signal returned to the baseline. The TPD spectrum was integrated and the number of moles of desorbed hydrogen determined by comparing to the areas of hydrogen pulses. Prior to experiments, the sample loop was calibrated with pulses of N_2 in a helium flow and compared against a calibration line produced from injections of N_2 using a gas tight syringe into a helium flow. It was found to be 51.9 μL.

After TPD of H_2, the sample was reoxidized at the activation temperature by pulses of pure O_2 in helium referenced to helium gas. After oxidation of the cobalt metal clusters, the number of moles of O_2 consumed was determined, and the percent reducibility determined assuming that the Co^0 reoxidized to Co_3O_4.

3. Results and Discussion

3.1 Al_2O_3 supported Catalysts

3.1.1 Support Effects

Figure 1 shows the TPR profiles for the unpromoted cobalt catalysts. For the two SiO_2 supported catalysts, two peaks emerged, attributed to the reduction of Co_3O_4 to CoO, which then reduces at higher temperatures to metallic Co^0, as observed previously for bulk cobalt [12]. As shown in the figure, the addition of surface ZrO_2 to silica did not significantly affect the reducibility, although there was a slight shift to higher temperatures. In addition to the two peaks observed for the Co/SiO_2 catalysts, the TiO_2 and Al_2O_3 supported cobalt catalysts displayed broad peaks at higher temperatures, due to the interaction of the CoO clusters with the support, which increased with decreasing cluster size.

3.1.2 Pt Promoter and Co Loading Effects

Figure 2 shows a TPR comparison of Pt promoted Co/Al_2O_3 with the unpromoted catalysts at two different loadings of cobalt 15% and 25%. Note that in the TPR, we did not ramp the temperature high enough to observe the reduction of cobalt aluminate species, which has been shown to occur above 1073 K with up to 30% loading of cobalt [13]. Therefore, the broad peak on the unpromoted catalyst (ca. 700 to 1000 K) is attributed to the reduction of CoO to Co^0, and the different shoulders being due to varying degrees of interaction with the support that is a function of the cluster size. The smallest CoO clusters, with the highest interaction with the support, therefore, are likely represented by the 950 K shoulder. The addition of Pt caused the peaks to shift markedly to lower temperatures, presumably due to spillover of H_2 from the reduced promoter to reduce the Co oxide species. Of particular importance, peaks attributed to the CoO-Al_2O_3 support interaction [14] are reduced at lower temperatures (ca. 50 K shift), freeing up the

availability of metal atoms for reaction. An increase in the cobalt surface phase with addition of Pt was observed in a previous investigation on Pt-Co catalysts for CO_2 reforming [15].

Results of H_2 chemisorption by TPD (Table 2) indicate that the number of surface sites increases with addition of the Pt promoter. By performing pulse reoxidation, it is clear that the remarkable gain in Co^o site density is mainly due to an enhancement in the reducibility of the cluster, and not to improvements in the actual dispersion (cluster size) of the reduced cobalt. However, for both the 15% and 25% cobalt catalysts, addition of Pt does cause a slight decrease in the cluster. This is reasonable, because the comparison was conducted at the same reduction temperature of 623 K, and addition of Pt should cause a fraction of the smaller CoO clusters that interact with the support to be reduced in this temperature range, resulting in a slightly smaller average cluster.

Interestingly, increasing the loading alone caused shifts in the reduction temperature of both the unpromoted and promoted catalysts, as observed previously [13]. With the unpromoted catalyst, for example, the maximum for the CoO to Co^0 peak shifted by 25K (from 850K to 825K), while the reduction of Co_3O_4 peak was only slightly affected. Results of H_2 chemisorption by TPD and pulse reoxidation (Table 2) revealed that, for both unpromoted and promoted catalysts, there were increases in the reducibility of the cluster by about 11-12% with a doubling of the cluster size. This is in agreement with a previous investigation [16].

3.1.3 Promoter Addition and Calcination Pretreatment Effects

The addition of Ru to the catalyst had a similar effect on the TPR as Pt. Figure 3 (left) shows that addition of 0.2% Pt results in a remarkable improvement in the reducibility for the catalyst, but that increasing promoter loading above 0.5% only resulted in marginal enhancement. As with the case of Pt, H_2 chemisorption (Table 2) shows that addition of Ru has a greater impact on the

cobalt reducibility than the dispersion, resulting in an almost twofold improvement in the number of active sites available for reaction after reduction at 623K while maintaining essentially the same average particle size.

For the case of Re, the reduction of Re occurs at higher temperatures than Pt or Ru. This is clearly shown in Figure 3 (right). Although there appears to be no improvement in the reduction of low temperature peak assigned to the reduction of Co_3O_4, Re still plays a valuable role in reducing the reduction temperature of CoO species for which there is a significant interaction of the cobalt metal with the support. A previous study of promotion of cobalt catalysts by Ref [12] found that rhenium on alumina reduced at approximately 698K, a value that falls between the two TPR peaks for the unpromoted Co-Al_2O_3 catalyst . Again, Table 2 shows by H_2 chemisorption that addition of Re improves the degree of reduction of the catalyst more than the dispersion (cluster size).

Figure 3 (right) shows profiles for two different series of Re promoted 15%Co/Al_2O_3 catalysts. The difference between the two series of catalysts is in the preparation. The dark line spectra correspond to catalysts prepared by loading the Co three times by successive incipient wetness impregnation steps, where the catalyst was dried between each impregnation step. Only one calcination was used after the last step. The other series of catalysts was prepared in a similar manner, except that the catalyst was calcined after each sequential impregnation and drying step, for a total of three times. Clearly, there is no advantage with respect to reducibility of using an interval calcination to prepare the catalyst.

Figure 4 provides a comparison of different Al_2O_3 supported cobalt catalysts with and without the addition of metal and metal cation promoters. Addition of noble metals aids in promoting the reduction rate. In contrast, as shown in Table 2, metal cations, ZrO_2 and La_2O_3, promote the

dispersion. With the ZrO_2-containing catalyst, the cobalt clusters were much smaller (Table 2). Therefore, it was expected that the interaction with the support (and perhaps the promoter cation) would be noticeably different in the TPR. Recall that the second peak corresponds to reduction of CoO to Co^0, and that the high temperature shoulder in the unpromoted catalyst is attributed to the interaction of smaller clusters with the support. Clearly, for the ZrO_2 promoted catalyst, there is a remarkable increase in the high temperature shoulder.

Also, for the ZrO_2 and La_2O_3 promoted samples, there was a noticeable lowering in the intensity of the peaks corresponding to reduction of CoO to Co^0 in comparison to the other samples. In considering the results in Table 2 for percent reducibility, it is presumed that the rest of the cobalt is present as aluminates, or perhaps some other mixed oxide form including the promoter, that reduces above 1073K. This correlates well with a previous study [13] in which decreasing cobalt loading (and presumably, cluster size) changed the ratio of peaks corresponding to oxide to aluminates in favor of aluminates. Another investigation, where different atomic contents of Co and Pt were used, yielded similar findings [17].

3.1.4 Cluster Resistance to Reduction Treatment

Table 3 shows the results of an experiment where the catalyst was ramped by 1K/min to a desired reduction temperature, and then held for 10 h for reduction in hydrogen. The catalyst was then cooled to 373K and ramped by 10K/min to the treatment temperature in inert gas to desorb the chemisorbed H_2. Each TPD of H_2 was followed by pulse reoxidation. This proceeded in a stepwise manner for reduction temperatures of 473K, 573K, 673K, 773K and 873K. Afterwards, a fresh sample was analyzed by ramping directly to 873K by 1K/min and reduced for 10 h at 873K. TPD and pulse reoxidation were conducted in the same manner. The data in Table 3 demonstrate that the cluster size does not change significantly for reduction at each temperature.

Rather, pulse reoxidation reveals that the percentage reduction changes at each step, increasing greatly the number of sites available for reaction. Changing the heating rate (direct heating versus slow ramp and hold) may cause some growth of the cluster (6.2 for direct versus 5.6 for ramp and hold). It appears that the smaller particles are being reduced using the ramp and hold procedure as the temperature is increased since there is a progressive decrease in average particles size: 5.9,073 K; 5.6, 773 K; 5.2, 873 K.

3.2 SiO_2, ZrO_2 modified SiO_2, and TiO_2 supported Catalysts

In contrast with the Al_2O_3 supported catalysts, there appeared to be little interaction with the support for these catalysts. This may be due to the much larger cluster size of the cobalt, as determined by H_2 chemisorption and pulse reoxidation (Table 4). Addition of either Ru or Pt to the support had a similar effect by decreasing the reduction temperature of the cobalt, as shown in Figure 5. Both promoters had a more important role in increasing the rate of reduction of the first peak that corresponds to Co_3O_4 to CoO. On an atom of promoter per atom of Co basis, Figure 5 indicates that Pt was more effective than Ru in enhancing the reduction of Co. In both cases, 0.005% (molar) loading of promoter was optimal for a catalyst with a loading of 15% Co. H_2 chemisorption and pulse reoxidation results indicated that the cluster size decreased remarkably with percent reducibility with the addition of noble metal promoters. It is likely that the increased reducibility allows for the reduction of cobalt-silicates [18-20] causing a decrease in the average cluster size. Adding a larger amount of noble metal promoter showed little further improvement in reduction. Addition of metal cation, K^+, led to shifts in both reduction peaks to higher temperatures, with a noticeable broadening of the peaks (Figure 6).

Figure 7 shows that similar promoter effects were observed with the ZrO_2-SiO_2 and TiO_2 supported Co catalysts as shown for Al_2O_3 and SiO_2 supports. Ru and Pt particularly enhanced

the rate of reduction for the first peak for all supports, and for the second peak when a significant metal-support interaction was present (Al_2O_3 and TiO_2 catalysts). A moderate enhancement was achieved for Pt and Ru promotion for the ZrO_2-SiO_2 catalyst for the second peak, while only a slight shift was observed for the promoted SiO_2 catalysts.

In all cases, Re had the opposite effect. Re played a more important role in catalyzing the reduction of the second peak, attributed to reduction of CoO to Co^0, particularly when a strong interaction of the support was present (Al_2O_3 and TiO_2 supported catalysts). The first peak changed very little or not at all for all supported catalysts studied.

References

1. Knifton, J.F., Lin, J-J, U.S. Patent 4,366,259 (Dec, 1982).
2. Beuther, H., Kibby, C. L., Kobylinski,T. P., Pannell, R. B., U.S. Patent 4,413,064 (1983).
3. Beuther, H., Kibby, C. L., Kobylinski,T. P., Pannell, R. B., U.S. Patent 4,493,905 (1985).
4. Kobylinski, T. P., Kibby, C. L., Pannell, R. B., Eddy, E. L., U.S. Patent 4,605,676 (1986).
5. Beuther, H., Kobylinski, R. B., Kibby, C. L., U.S. Patent 4,585,798 (1986).
6. Iglesia, E. Soled, S. L., Fiato, R. A., U.S. Patent 4,738,948 (1988).
7. Iglesia, E. Soled, S. L., Fiato, R. A., U.S. Patent 4,822,824 (1989).
8. Iglesia, E. Soled, S. L., Fiato, R. A., and Via, G. H., *J. Catal.* **143** (1993) 345.
9. Bruce, L. A., Hoang, M., Hughes, A. E., and Turney, T. W., *Appl. Catal. A*, **100** (1993) 51.
10. Iglesia, E., Soled, S. L., Baumgartner, J. E., and Reyes, S. C., *J. Catal.* **153** (1995) 108.
11. Vada, S., Hoff, A., Adnanes, E., Schanke, D., and Holmen, A., *Topics in Catal.* **2** (1995) 155.
12. Hilmen, A.M., Schanke, D., and Holmen, A., *Catal. Lett.* **38** (1996) 143.
13. Wang, W-J, and Chen, Y-W, *Appl. Catal.* **77** (1991) 223.
14. Ji, L., Lin, J., and H.C. Zeng, J. Phys. Chem. B **104** (2000) 1783.

15. Tang, S., Lin, J., and Tan, K.L., *Surf. Interface Anal.* **28** (1999) 155.

16. Reuel, R.C. and Bartholomew, H., *J. Catal.* **85** (1984) 63.

17. Moraweck, B., Frety, R., Pecchi, G., Morales, M. and Reyes, P., *Catal. Lett.* **43** (1997) 85.

18. Reinikainen, M., Niemala, M.K., Kakuta, N., and Suhonen, S., *Appl. Catal.* **174** (1998) 61.

19. Riva, R., Miessner, H., Vitali, R., and del Piero, G., *Appl. Catal.* **196** (2000) 111.

20. Bazin, D., Kovacs, I., Guczi, L., Parent, P., Laffon, C., de Groot, F., Ducreux, O., and Lynch, J., *J. Catal.* **189** (2000) 456.

Table 1 BET Surface Areas				
Catalyst	BET SA (m^2/g)	+/-	Avg. Pore Size (nm)	Calcination T (K)
15%Co/Al_2O_3	157.7	0.2	4.2	673, flow
15%Co-0.5%Pt/Al_2O_3	161.6	0.2	4.1	673, flow
15%Co-1%Ru/Al_2O_3	159.1	0.2	3.1	673, flow
15%Co-1%Re/Al_2O_3	187.7	0.2	4.0	673, flow
15%Co-5%La/Al_2O_3	155.1	0.2	3.9	673, flow
15%Co-15%Zr/Al_2O_3	160.9	0.1	4.1	673, flow
15%CoSiO_2	217.1	0.7	7.7	673, no flow
15%Co-3.83%Pt/SiO_2	217.0	0.6	7.3	673, no flow
15%Co-2%Ru/SiO_2	208.9	0.5	7.6	673, no flow
15%Co-0.5%K/SiO_2	210.9	0.5	7.9	673, no flow
20%Co/Zr-SiO_2	200.0	0.6	8.8	673, flow
20%Co-0.5%Pt/Zr-SiO_2	205.5	0.6	9.2	673, flow
20%Co-0.5%Ru/Zr-SiO_2	197.0	0.6	8.4	673, flow
20%Co-0.5%Re/Zr-SiO_2	191.9	0.6	8.9	673, flow

Table 2

H_2 Chemisorption (TPD) and Pulse Reoxidation Results for Al_2O_3 Supported Catalysts, With and Without Promoter

Sample Name	Red. T (K)	μmoles H_2 desorbed per g cat	Uncorr. %D	Uncorr. Diam. (nm)	μmoles O_2 Pulsed per g	% Red.	Actual %D	Actual Diam. (nm)
15%Co/Al_2O_3	623	66.9	5.3	19.6	509	30	17.5	5.9
15%Co-0.5%Pt/Al_2O_3	623	140.6	11.0	9.3	1024	60	18.4	5.6
15%Co-1%Ru/Al_2O_3	623	115.5	9.7	11.4	823	50	18.2	5.7
15%Co-1%Re/Al_2O_3	623	168.2	13.2	7.8	1187	70	19.4	5.5
15%Co-5%La/Al_2O_3	623	59.8	4.7	22.0	450	27	19.1	5.4
15%Co-15%Zr/Al_2O_3	623	45.5	3.6	28.9	195	11	32.4	3.2
25%Co/Al_2O_3	623	77.7	3.7	28.2	1174	42	8.7	11.8
25% Co-Pt/Al_2O_3	623	149.0	7.0	14.7	1994	71	9.4	11.0

Table 3

Resistance of Cluster to Reduction Temperature and Heating Rate. Results of H_2 Chemisorption by TPD

Sample Name	Red. T (K)	μmoles H_2 desorbed per g cat	Uncorr. %D	Uncorr. Diam. (nm)	μmoles O_2 Pulsed per g	% Red.	Actual %D	Actual Diam. (nm)
15%Co/Al_2O_3	473	26.3	2.1	49.9	---	---	---	---
	573	38.6	3.0	34.0	232	14	22.3	4.6
	673	77.6	6.1	16.9	462	27	22.3	5.9
	773	131.8	10.4	10.0	953	56	18.4	5.6
	873	152.8	12.0	8.6	1021	60	19.9	5.2
15%Co/Al_2O_3*	773	122.2	9.6	10.8	971	57	16.8	6.2

*Direct temperature ramp.

Table 4

Sample Name	Red. T (K)	μmoles H_2 desorbed per g cat	Uncorr. %D	Uncorr. Diam. (nm)	μmoles O_2 Pulsed per g	% Red.	Actual %D	Actual Diam. (nm)
15%Co/SiO_2	623	16.9	1.3	77.6	1078	64	2.1	49.7
15%Co-Pt/SiO_2	623	25.0	2.0	52.5	1222	72	2.7	37.8
15%Co-Ru/SiO_2	623	37.8	3.0	34.8	1249	74	4.0	25.7
15%Co-K/SiO_2	623	17.9	1.4	73.2	994	59	2.0	51.1
20%Co/Zr-SiO_2	623	47.6	2.8	36.8	1149	51	5.5	18.8
20%Co-Pt/Zr-SiO_2	623	59.0	3.5	29.7	1207	53	6.6	15.7
20%Co-Ru/Zr-SiO_2	623	61.4	3.6	28.5	1247	55	6.6	15.7
20%Co-Re/Zr-SiO_2	623	59.0	3.5	29.7	1308	58	6.0	17.2
10%Co/TiO_2	573	42.8	5.1	20.0	593	52	9.7	10.6
10%Co-Ru/TiO_2	573	66.6	7.8	13.3	722	64	1.2	8.5
10%Co-Re/TiO_2	573	65.6	7.7	13.4	685	61	12.8	8.1
10%Co-B/TiO_2	573	37.4	4.4	23.5	429	38	11.6	8.9
10%Co-Ru-B/TiO_2	573	63.1	7.4	13.9	692	61	12.2	8.5

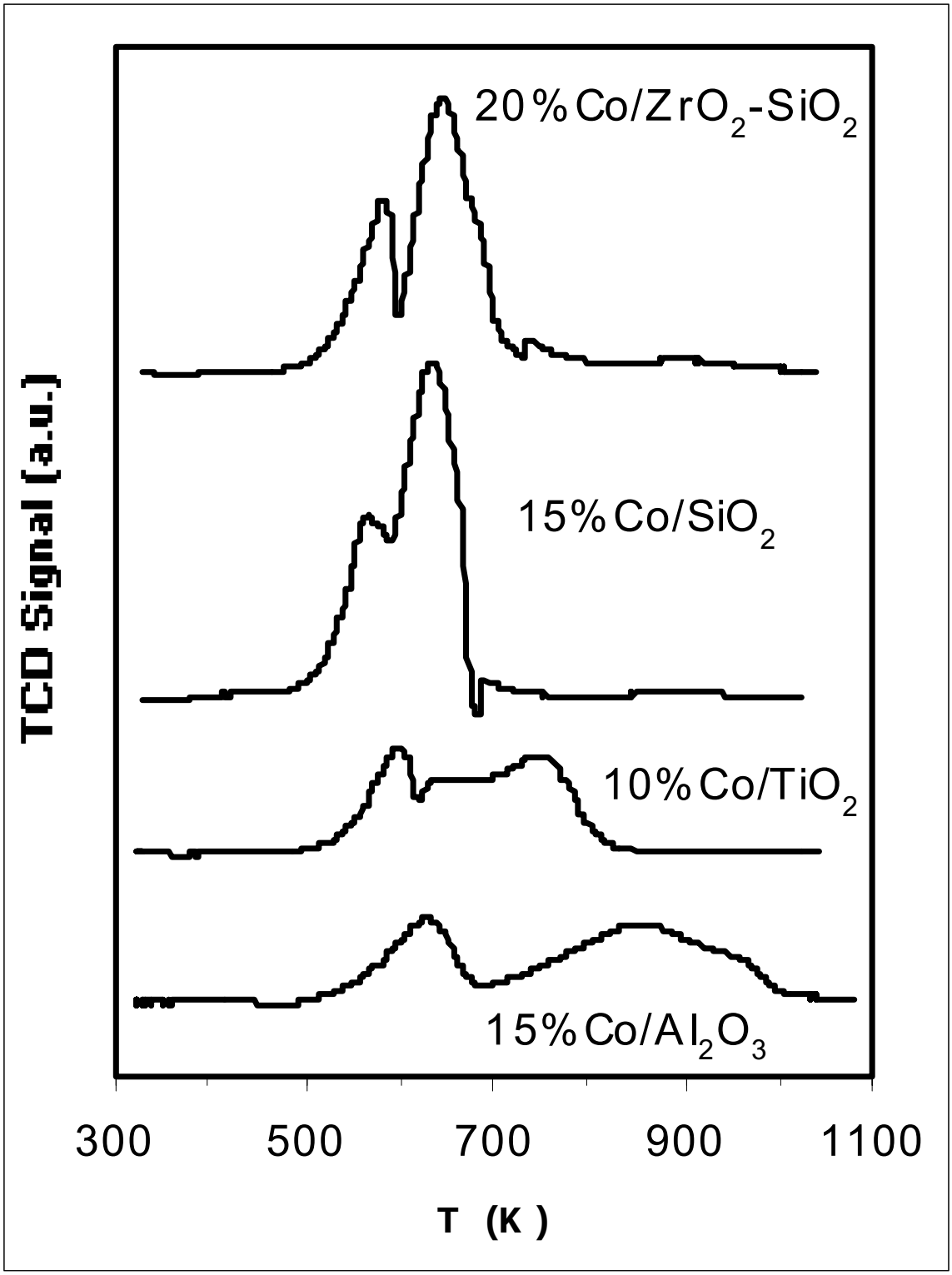

Figure 1. TPR of unpromoted Co catalysts.

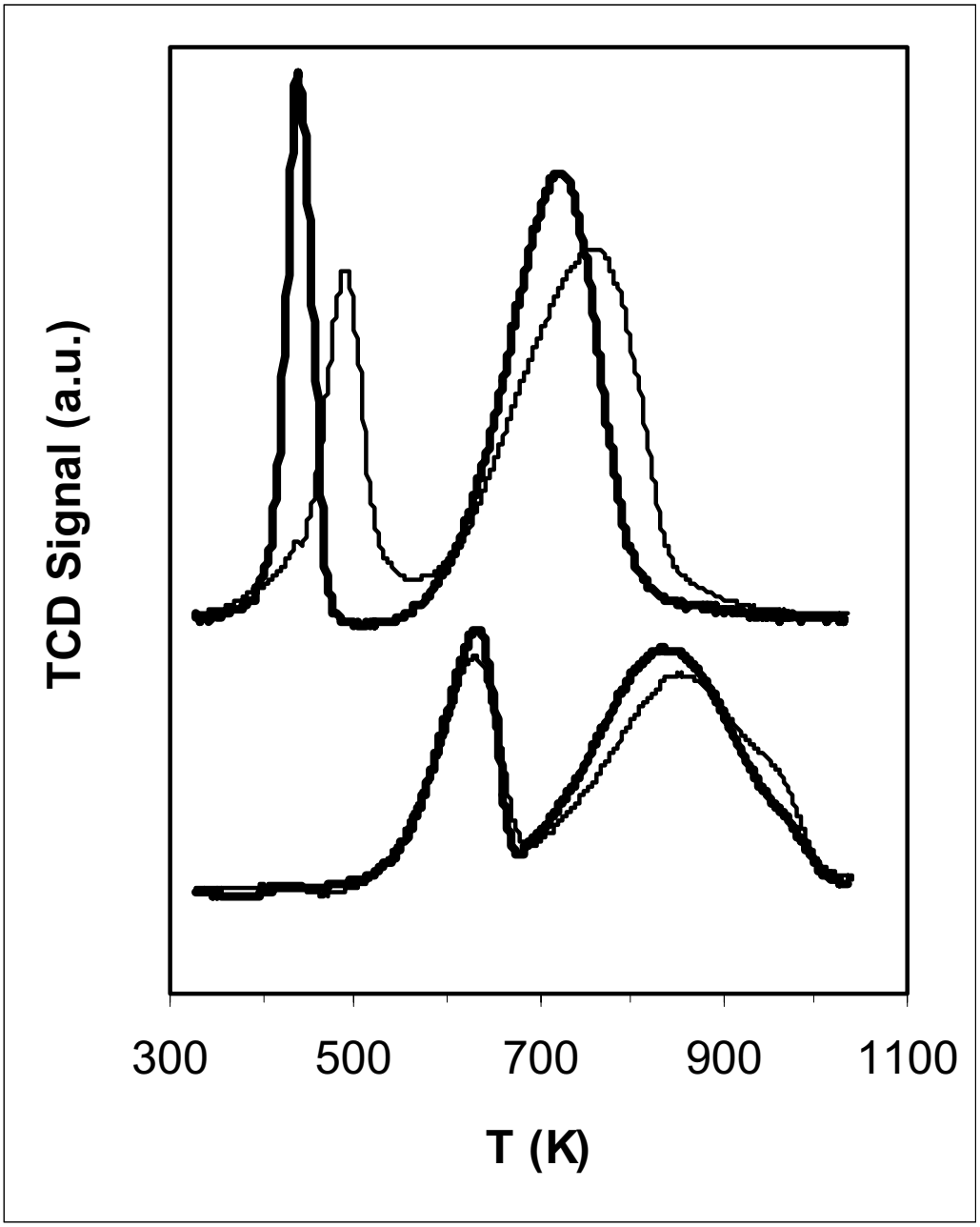

Figure 2. Comparison of unpromoted (bottom) and 0.5% Pt promoted (top) Co/Al_2O_3 FTS catalyst with 15% (bold) and 25% (light) loadings of Co. Note that the intensity of the 15% catalyst was increased by 1.7 to account for differences in loading in order to more easily compare shifts in the peak positions.

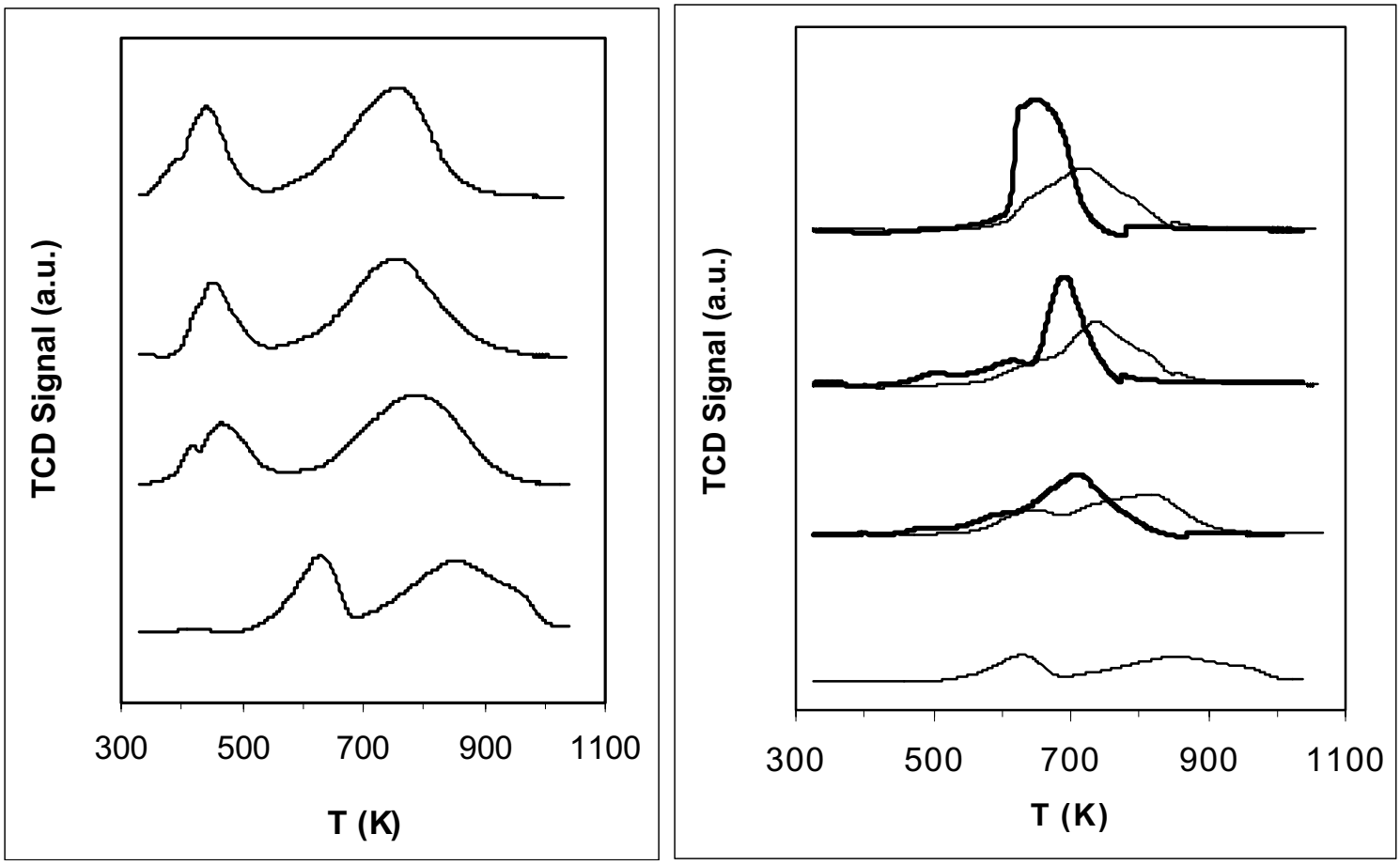

Figure 3. (left) Comparative TPR spectra of umpromoted (bottom) 15% Co/Al_2O_3 catalyst with those promoted with (bottom to top) 0.2%, 0.5% and 1.0% Ru, respectively. (right) Comparative TPR spectra of unpromoted (bottom) 15%Co/Al_2O_3 catalyst with those promoted with (bottom to top) 0.2%, 0.5% and 1.0% Re with (light) and without (dark) interval calcination.

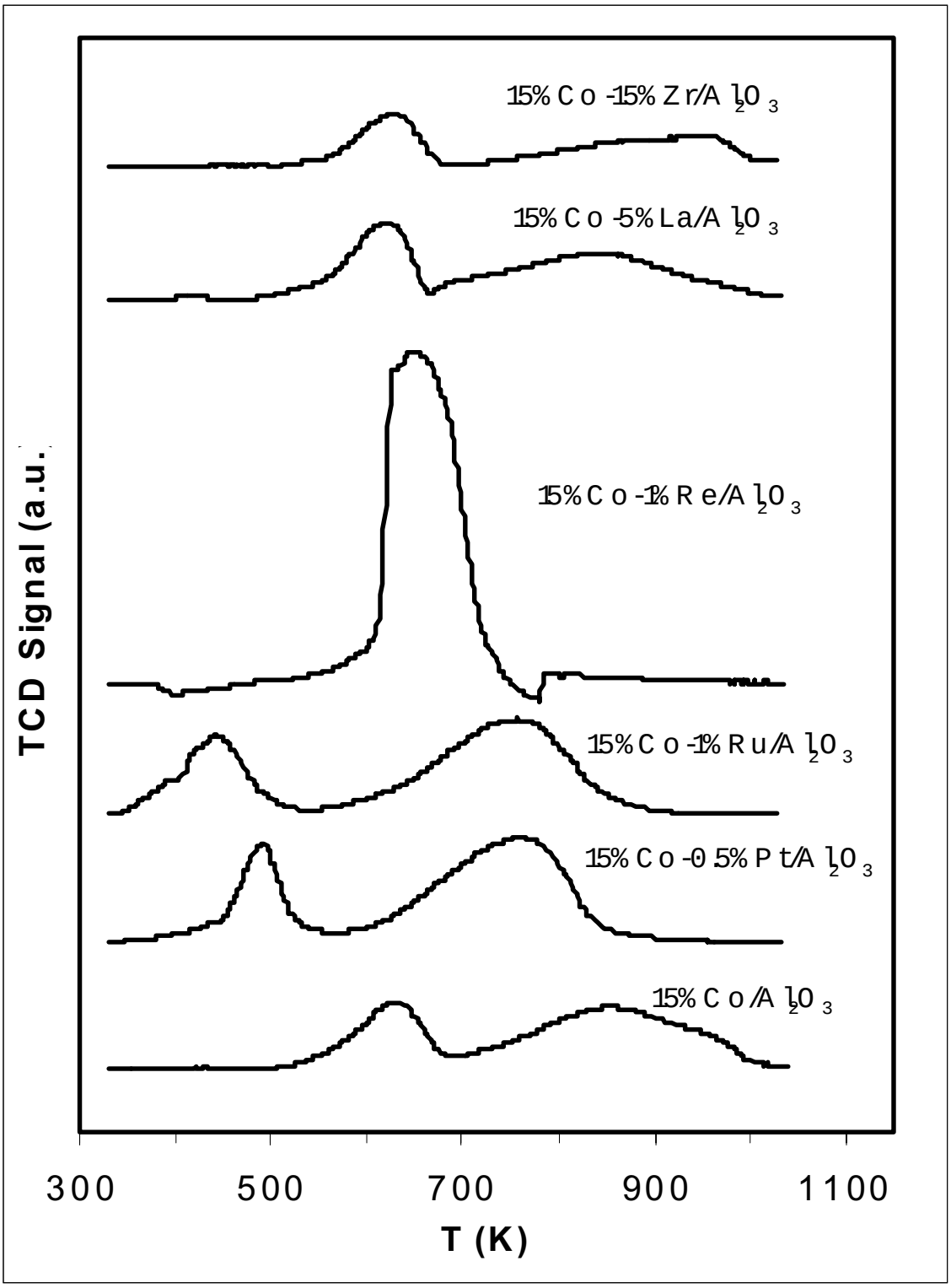

Figure 4. TPR comparison of Al_2O_3 supported Co catalysts with and without metal and metal cation promoters.

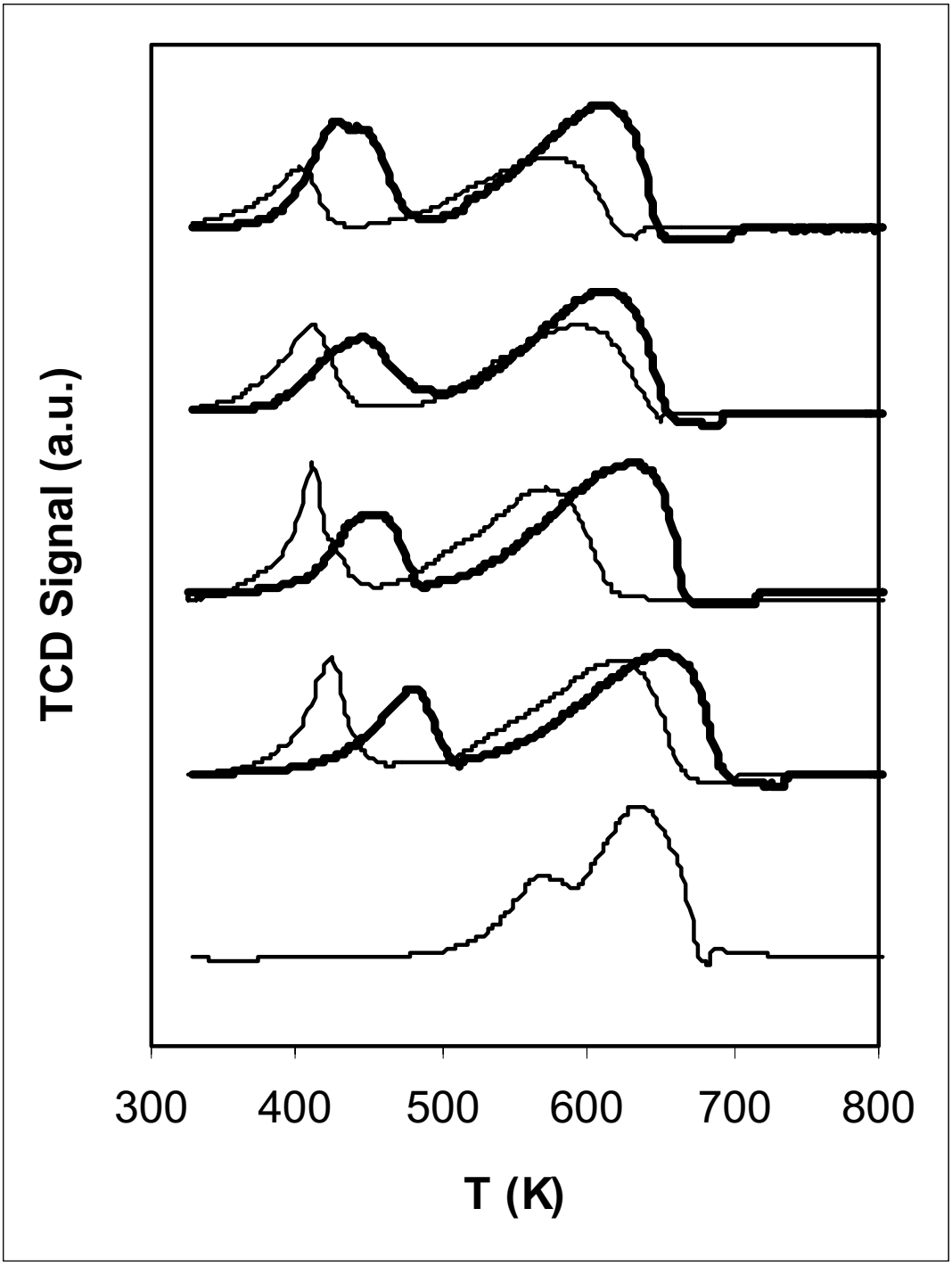

Figure 5. TPR comparison of unpromoted (bottom) and promoted SiO_2 supported Co catalysts with increasing molar percentages of Ru (bold) and Pt (light) in the order (moving p) 0.002%, 0.005%, 0.01% and 0.02%.

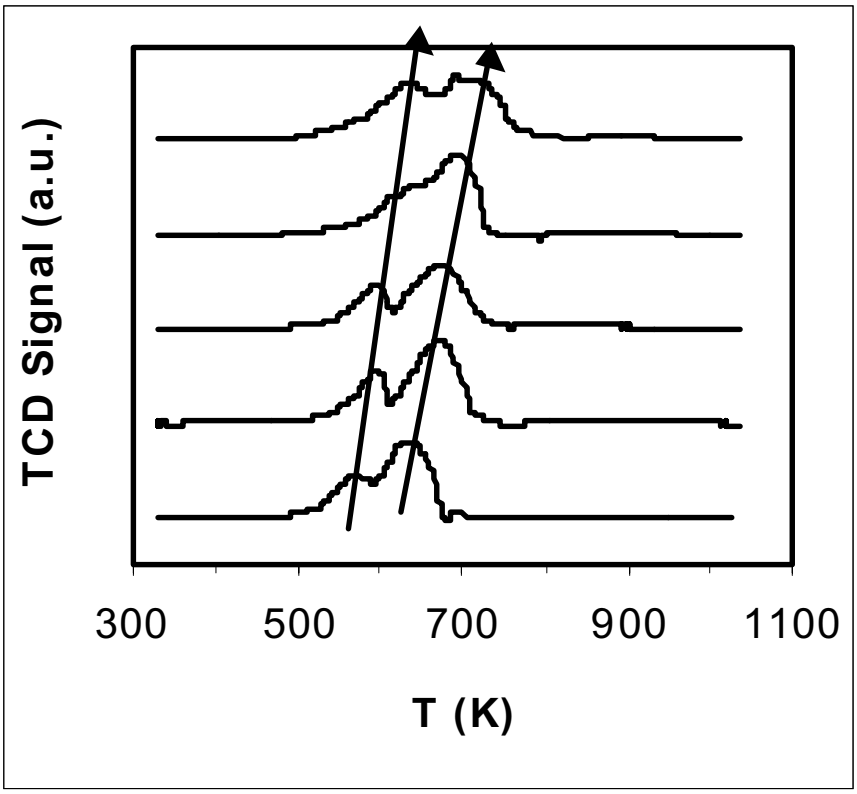

Figure 6. TPR comparison of unpromoted (bottom) and K^+ promoted SiO_2 supported Co catalysts with (moving up) increasing wt.% loading of K^+ in the order 0.5%, 1.5%, 3.0% and 5.0%.

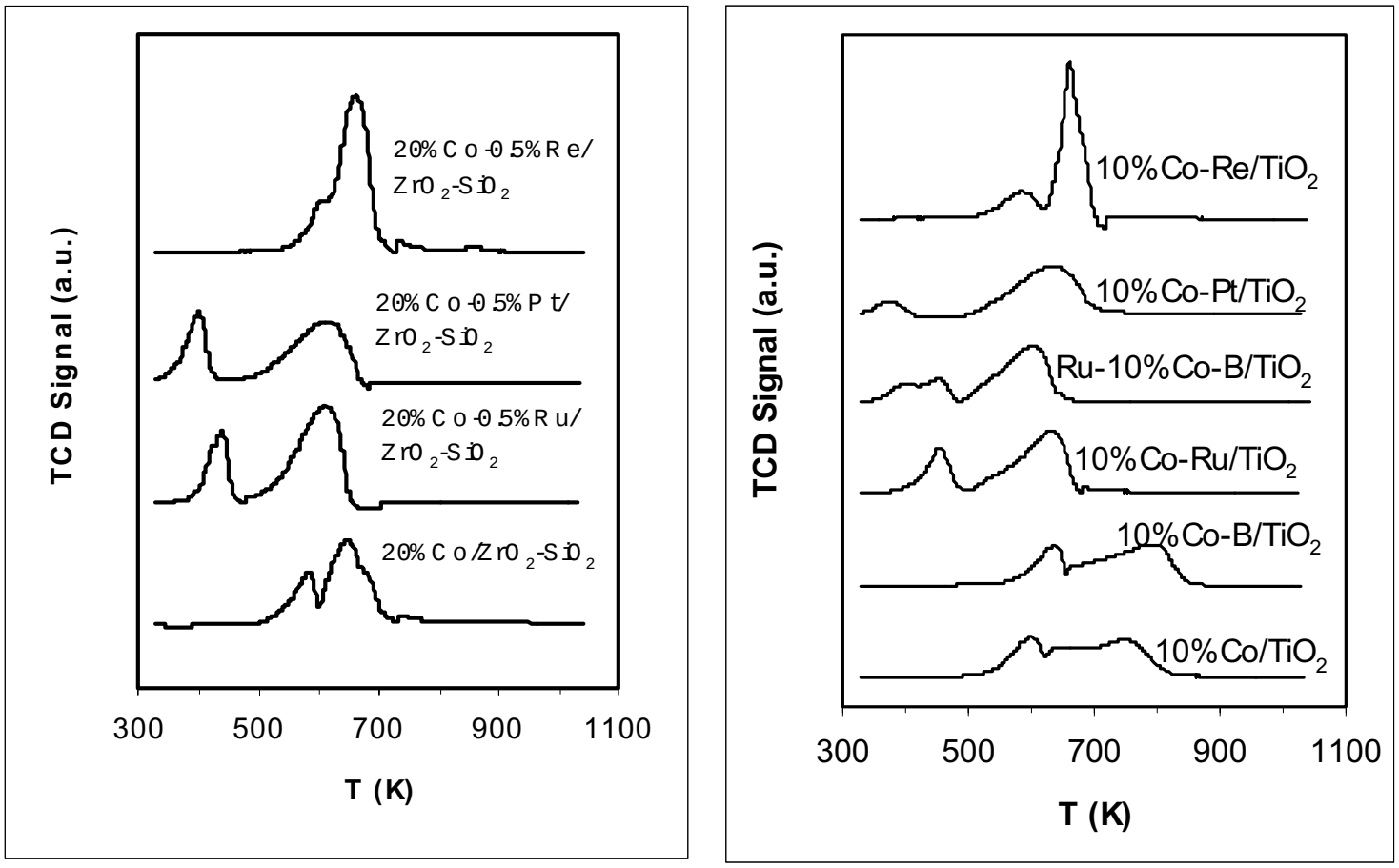

Figure 7. TPR comparison of promoted (left) ZrO_2-SiO_2 and (right) TiO_2 catalysts.

Task 4. Wax/Catalyst Separation

The objective of this task is to develop techniques for the separation of catalysts from FT reactor slurries.

A. Slurry Bubble Column Reactor (SBCR) Activities

Abstract

During this reporting period, the SBCR modifications detailed in the previous quarterly report, were completed. In this report we describe results and operating experiences for a 404-hour SBCR shakedown run that was completed in December. Special emphasis was placed on maintaining a constant catalyst within the reactor vessel while reducing slurry holdup within the wax separation system. A new system for measuring the SBCR slurry level using a differential pressure transducer was implemented and thoroughly tested. The differential pressure signal was also found to give important information regarding the liquid recirculation rate and gas holdup within the reactor system.

Activity decline of an iron-based FT catalyst during the shakedown run was documented and compared with that of previous CSTR and SBCR runs using the same catalyst and operating conditions. The activity decline measured in the revamped SBCR system was shown to be similar to that of the CSTR experiments.

Introduction

A Slurry Bubble Column Reactor (SBCR) is a gas-liquid-solid reactor in which the finely divided solid catalyst is suspended in the liquid by the rising gas bubbles. SBCR offers many advantages over fixed-bed type reactors such as: 1) improved heat transfer and mass transfer; 2) an isothermal temperature profile is maintained; and 3) relatively low capital and operating cost. Fischer-Tropsch Synthesis (FTS) takes place in a SBCR where the synthesis gas is

converted on catalysts suspended as fine particles in a liquid. The synthesis gas flows in a bubble phase through the catalyst/wax suspension. The bubbles in the catalyst slurry are produced by a gas distributor in the bottom of the reactor. The volatile products are removed with unconverted gases, and the liquid products are separated from the suspension.

A considerable interest has been expressed in using the SBCR for FTS specifically for the conversion of stranded natural gas into liquids. Currently, the CAER is using the Prototype Integrated Process Unit (PIPU) system for scale-up research of the FTS.

As discussed in the previous report, the CAER 5.08 cm diameter SBCR plant was overhauled and redesigned to incorporate automatic slurry level control and wax filtration systems. These design changes allow a more constant inventory of the catalyst to be maintained in the reactor while reducing slurry hold-up in the catalyst/wax separation system. In addition, the wax filtration system was rearranged to accept a variety of filter elements. These additions were meant to enhance the stability of the reactor operation so that long-term tests can be conducted to study catalyst deactivation and attrition under real-world conditions.

In the following discussion, we will detail the results and operational experiences of a shakedown run with the enhanced SBCR system. Objectives of the shakedown were to: 1) test the new slurry level control system; 2) compare the performance of a precipitated Fe/K Fischer Tropsch Synthesis (FTS) catalyst in the enhanced SBCR and a continuous stirred tank reactor (CSTR); and 3) determine the effectiveness of the catalyst/wax filtration system.

Experimental/Summary of Design Modifications

The SBCR apparatus, shown in Figure 1 (1), was originally designed as a direct coal liquefaction reactor. In the current configuration, the bubble column has a 5.08 cm diameter and a 2 m height with an effective reactor volume of 3.7 liters. The synthesis gas was passed

continuously through the reactor and distributed by a sparger near the bottom of the reactor vessel. The product gas and slurry exit the top of the reactor and pass through an overhead receiver vessel where the slurry is disengaged from the gas-phase. Vapor products and unreacted syngas exit the overhead vessel, enter a warm trap (100°C), and then a cold trap (3°C). A dry flow meter down-stream of the cold trap was used to measure the exit gas flow rate.

A dip tube was added to the reactor vessel so that the F-T catalyst slurry could be recycled internally via a natural convection loop. The unreacted syngas, F-T products, and slurry exited into a side port near the top of the reactor vessel and entered a riser tube. The driving force for the recirculation flow was essentially the difference in density between the fluid column in the riser (slurry and gas) and that of the dip-tube (slurry only). The dip tube provided a downward flow path for the slurry without interfering with the upward flow of the turbulent syngas slurry mixture. Thus, to some degree, back mixing of the slurry phase and wall effects in the narrow reactor tube were minimized.

During the period from 1995-96, attempts to operate the direct liquefaction reactor in a F-T mode were successful in that a clear wax product could be obtained. However, the initial activity observed in the bubble column was about 10-15% less than that of comparable CSTR runs. Also, the rate of conversion decline (and apparent catalyst deactivation) in the SBCR was much greater than that observed in the CSTR. As detailed in the previous report (1), it was hypothesized that the apparent increased deactivation rate in the SBCR was caused by the depletion of catalyst inventory due to the nature of the wax/catalyst separation system.

Based upon the analysis of the previous SBCR runs (in 1995-96), several more design changes were carried out to the SBCR system to increase the conversion stability. An automatic level controller was added to the overhead slurry/gas separation tank. This insured that a constant

inventory of catalyst particles was being maintained in the reactor vessel when the superficial gas velocity within the column was constant.

Originally, the overhead separator vessel was designed to enhance settling of the catalyst particles. Thus, wax separation from the slurry was to be extracted near the top of the vessel where the catalyst concentration would be lower than that near the bottom. Unfortunately, this approach required a large hold-up volume of slurry outside the reactor (greater than the reactor volume itself). Hold-up of slurry outside the reactor was lowered by decreasing the volume of the overhead vessel from 18 to 4 liters.

The sintered metal filter tube was moved to the liquid downcomer below the overhead separation vessel. Currently, the filter is a flow-through device having a sintered metal tube in a shell. Filtered wax was extracted radially through the tube while slurry flows downward in the axial direction. The shear force of the axial slurry flow appears to prevent excessive caking of the catalyst around the filter media. Filtered wax was metered into a storage tank through a let-down valve operated by the overhead liquid-level controller. Pressure drop across the filter media can be varied manually by varying the wax storage tank pressure. The filter assembly was configured such that the filter media could be replaced on-line, without aborting or interrupting the reactor run.

The level or volume of the slurry within the receiver was continuously monitored by measuring the differential pressure across the height of the vessel. Argon was purged through each of the pressure legs to keep the lines free of slurry. Slurry volume within the receiver was controlled to be no more than 1.3 liters by removing wax from the reactor system via the level control valve. The unfiltered slurry flowed back to the reactor via a natural convection loop through a dip-tube exiting near the bottom of a reactor.

Catalyst Activation and SBCR Startup Procedure. In preparation for catalyst activation , the SBCR was filled with 2.8 liters (~75% of the reactor volume) of a slurry consisting of 20 wt% iron catalyst and Shell C_{30} oil. An additional 1.3 liters of the C_{30} oil was isolated in the overhead separation vessel. The reactor was pressurized with flowing CO gas at 175 psig (12 atm) while the slurry temperature was increased to 270°C at a 50°C/ hour rate. Once the reactor temperature stabilized at 270°C, the exit gas was periodically monitored for CO_2 to observe the progress of activation, (see Figure 2). During the activation period, the down-comer leg from the overhead vessel to the reactor was valved-off so that the catalyst remained isolated inside the reactor. Likewise, the C_{30} oil in the overhead vessel did not mix with reactor catalyst during activation.

After the catalyst had been activated (~24 hours), hydrogen gas flow was phased in with the CO feed gas. Once the desired gas space velocity had been attained, the down-comer valve used to isolate the C_{30} oil in the overhead vessel was opened to allow circulation between the reactor, riser and down-comer legs. Once the C_{30} oil became mixed with the activated catalyst slurry and the reactor temperatures were stabilized, CO, H_2, and syngas conversions were calculated at least once a day to monitor the reactor performance.

Discussion of Results

Gas Hold-up. Gas hold-up, ϵ_g , is a useful parameter for predicting both the flow and mass transfer dynamics within SBCR reactors (2). Additionally, with the current SBCR configuration, the fraction of reactor volume occupied by gas was needed to determine the gas space velocity on a per gram of catalyst basis. Slurry volume within the reactor was not directly measured. Instead, only slurry occupying the overhead separator vessel was measured via a differential pressure transmitter. The reactor vessel was always flooded with slurry/gas, provided a slurry level was

indicated in the overhead separator vessel; therefore, by knowing the gas holdup for any given superficial velocity, the mass of slurry within the reactor could be estimated by difference.

Before the shakedown run, a method for calculating ϵ_g was developed and tested using the C_{30} oil, without a catalyst. Approximately 5 liters of a Shell C_{30} oil product was loaded into the SBCR system. This quantity was sufficient to flood the reactor volume and partially fill the overhead vessel. The baseline liquid level in the overhead vessel was recorded without gas flowing through the reactor (i.e., $U_g = 0$). The SBCR was pressurized with Argon gas to 175 psig and the temperature increased to 270°C to simulate FTS run conditions planned for the shakedown run. The baseline liquid level was recorded again to note the expansion of the oil. Argon was introduced at superficial velocities ranging from 0.7 to 3 cm/s. The liquid level increase above the baseline level was effectively due to gas displaced in the reactor vessel. Therefore, the displaced liquid volume divided by the reactor volume was equal to ϵ_g. A similar procedure was also performed using the reactor loaded with 15 wt% catalyst suspended in product wax and syngas at the end of the shakedown synthesis run. The results of both the C_{30} oil and slurry holdup tests are plotted in Figure 3. For any given Ug, the gas holdup during FT synthesis was lower than that with C_{30} oil only. This phenomenon was due to the gas contraction experienced in the reactor from the conversion of syngas to liquid products. Additionally, the solids content in the wax slurry tended to increase the effective viscosity, thus lowering ϵ_g (3).

SBCR Shakedown/Conversion Comparisons between CSTR and SBCR runs. One of the objectives of the shakedown run was to compare the performance of the enhanced SBCR performance with the previous SBCR configuration. It was anticipated that the modified SBCR system performance, in terms of catalyst deactivation, would be comparable to that of the CSTR

experiments. The shakedown run/activation conditions for the enhanced SBCR system along with the comparison SBCR and CSTR conditions are listed in Table 1.

The gas conversions versus time-on-stream for the enhanced SBCR are displayed in Figure 4. A gas space velocity of 5.3 slph/g was used during the initial startup period. CO conversion reached a maximum of 78% after 72 hours time-on-stream (TOS). After this catalyst induction period, the gas conversion started to steadily decline to about 72% after 192 hours TOS. Corresponding carbon dioxide and methane selectivities are shown in Figure 5. Carbon dioxide selectivity stabilized to 45% while the methane selectivity averaged 4%. The alpha plot and alkene selectivity distribution by carbon number for the 5.3 slph/g space velocity period are displayed Figures 6 and 7, respectively. The short duration of the shakedown run was not sufficient to purge the system completely of the C_{30} startup oil, as evidenced by the protuberance in the alpha plot near n=28-32.

After 192 hours on stream, the space velocity was increased to 5.8 slph/g due to difficulties experienced with syngas flow instrumentation. The syngas H_2/CO ratio was increased to 2.0 after 240 hours TOS to check the additional capabilities of the SBCR system. This resulted in a precipitous drop in gas conversion and significantly lowered the production rate of heavy waxes to point where the slurry level in the overhead separation vessel was depleted after only 24 hours. As shown in Figure 5, the selectivity was shifted toward lighter products such as methane. At this point, it was decided to reactivate the catalyst with CO gas for 24 hours and subsequently return to the starting run conditions. Gas conversion increased substantially after reactivation; however, problems with establishing recirculation and a measurable liquid level continued. Without an adequate liquid pressure head in the down-comer leg, the driving force for the natural convection loop was nonexistent. Thus, a one liter volume of C_{30} oil was added to the system 48

hours after reactivation to promote slurry recirculation. This was effective in increasing the gas conversion and returning characteristic recirculation pattern to the overhead level signal.

The CO conversion data obtained from the enhanced bubble column (SBCR-JKN), the older SBCR configuration (SBCR-LGX) and CSTR under similar run conditions is displayed in Figure 8. Significant differences in conversion between the two SBCR configurations are apparent. The enhanced SBCR (run # SBCR-JKN) conversion continued to increase after +70 hours. The older SBCR (run # SBCR-LGX) conversion continued to drop at a significant rate after activation and was consistently lower than that of the CSTR and enhanced SBCR.

Slurry back-mixing in the enhanced SBCR is significantly reduced by the addition of the down-comer/dip-tube flow path; consequently, the gas and liquid phases likely exhibited more "plug-flow" behavior. Thus, for a given space velocity, the enhanced SBCR should yield a higher conversion than that of a CSTR (4). Differences in conversion between the two reactor types may also be caused by the dissimilarity of heat and mass transfer phenomena.

Catalyst Deactivation Rate Comparisons. Catalyst deactivation rates were compared between the different reactor configurations using the activity function defined as:

$$a(t) = \frac{r_{FT}(t')}{r_{FT}(t'=0)} \approx \frac{X_{CO}(t')}{X_{CO}(t'=0)}.$$

Where t′ is the time after attaining the maximum total reaction rate or conversion. The maximum reaction rate was identified for each conversion curve, as shown in Figure 8. The relative activity functions were calculated from the maximum conversion and plotted in Figure 9 versus the relative t′ time-scale. In this fashion, each of the deactivation rates could be compared on an equal basis, independent of the conversion levels.

The deactivation rates calculated for the SBCR-JKN and CSTR cases followed a linear zero order fashion with decay constants of 0.0130 and 0.0142 day $^{-1}$, respectively. The apparent catalyst activity decline of the SBCR-LGX appeared to have two distinct rate deactivation periods: a relative rapid decay of 0.0624 day $^{-1}$ followed by another linear decay period with a slope of 0.0156 day^{-1}. This second decay period was apparently due to a transient effect from the accumulation of catalyst within the large overhead vessel and filtering system. Thus, the decrease in reaction rate and conversion during this initial decay period was caused by a steady increase in the space velocity as catalyst was removed from the reactor. Once the SBCR-LGX system reached steady-state, the activity decline rate was comparable to the other reactor configurations.

Level Control and Slurry Recirculation. While the level sensing instrumentation for the overhead receiver was being modified, the level controller was operated in the manual mode. Since a low-alpha catalyst was used on this first run, wax production was low (<300 g per day), yielding a level increase in the overhead receiver of only ~1" per day. Therefore, daily manual letdowns were sufficient to maintain ~1 liter of slurry in the vessel. After the modifications were completed, the controller was allowed to operate the letdown valve as required to maintain the desired liquid level.

A typical recorder trace of the overhead receiver level is presented in Figure 10. The signal varies by as much as $\pm$ 0.75" w.c. due to the small pressure perturbations caused by gas bubbles traveling up the reactor, with the pressure signature of these bubbles being transferred to the overhead receiver via the diptube. To prevent these transient level indications from influencing the level controller, the controller operated using ten minute average values.

It was quickly learned that this recorder trace was a reliable indicator for the loss of recirculation. Figure 10 illustrates such an upset, with the width of the trace instantaneously

narrowing with the loss of recirculation. Three thermocouples monitoring the surface temperature at various points on the recirculation loop also helped confirm this, but were somewhat slower to react.

A few instances of operator-induced loss of recirculation occurred early in the run because of draining the warm and cold traps too rapidly, thus unduly upsetting the system pressure, but these were soon eliminated as experience was gained. However, most of these upsets were spontaneous and two scenarios have been espoused to explain them. One possibility is that the interruptions were caused by gas bubbles forming inside the reactor dip-tube, which would have reduced the pressure difference that is the driving force between the riser and the down-comer. A second possibility is that a filtercake was being formed on the inner surface of the filtration tube during letdown, which partially blocked the down-comer.

Following a loss of recirculation, the flow was often reestablished without operator intervention, but the recovery time varied. Recirculation flow was restarted by two methods. Momentarily increasing the syngas flowrate by ~20% was usually sufficient to reestablish recirculation, but occasionally a more vigorous action was used. The overhead receiver was isolated and pressurized with argon to ~150 psi above the normal system pressure. Venting the pressure via the down-comer then forced the presumed filter cake or gas bubbles down the reactor diptube. The riser block valve was then quickly opened, reestablishing recirculation.

Figure 11 is a trace of the overhead receiver level signal during a spontaneous loss of recirculation and recovery via the pressurization method. In this figure, time is plotted right to left, with each vertical line representing 15 minutes. After ~45 minutes without recirculation, the operators intervened and reestablished flow in the recirculation loop. The subsequent step change

in the signal was due to readjusting the argon purge flow to the differential pressure cell measuring the liquid level.

Overall, the level control system was effective in maintaining a relatively constant inventory of solids within the reactor. The wax filtration system produced a clean wax with virtually no signs of media plugging during the +400 hours of continuous operation. The level indication/control system was robust and effective in maintaining a steady inventory of catalyst slurry in contact with the gas-phase. The recorder trace of the overhead receiver liquid level was a reliable qualitative indicator of the slurry recirculation rate.

Dispersion of Catalyst within the SBCR System. The current SBCR system requires a relatively even distribution of the catalyst within the recirculation loop. Since about 25% of the slurry was flowing outside the reactor at any given instant, compensating for this characteristic to accurately calculate the space velocity was necessary (the cited space velocities were based only on the mass of catalyst residing in the reactor).

At the conclusion of the run, slurry samples were extracted from four locations in the SBCR system: 1) the bottom of the overhead separation vessel; 2) the bottommost reactor port, adjacent to the gas sparger; 3) gas-liquid riser; and 4) the lower-middle reactor port, located about 0.3 meters above the gas sparger. The samples were analyzed for catalyst solids using a standard ASTM ash content procedure, the results of which are displayed in Table 2. In general, the weight percent of catalyst solids in the slurry at the highest elevations (riser and overhead vessel sample points, 10.42 and 10.93 wt%, respectively) outside the reactor were lower than nominal 15 wt% catalyst loading concentration.

Conclusions

A shakedown experimental run of the CAER's enhanced SBCR was successfully completed. SBCR gas holdup (ϵ_g), was measured by recording the liquid level in the overhead separation vessel at

various superficial velocities through the reactor. Automatic control of the slurry level was both robust and effective in maintaining a constant catalyst inventory in the reactor. Differential pressure fluctuations from the level controller provided qualitative information regarding the slurry recirculation rate. The catalyst slurry filter yielded a clean wax product with virtually no signs of media plugging during 400+ hours of continuous operation.

Measured deactivation rates in the enhanced SBCR system were comparable to that of CSTR experiments under similar conditions. Transient problems with a previous SBCR run were identified and corrected. Another series of pilot plant runs are scheduled starting January 2001. Future experimental work with SBCR will focus on high alpha catalysts, wax filter media and catalyst attrition studies.

Nomenclature

a(t) Catalyst activity function

k_d First order deactivation rate constant, day^{-1}

$r_{F\text{-}T}$ Rate of Fischer-Tropsch synthesis, mole s^{-1} Fe·g $^{-1}$

SV Gas space velocity, Sl h^{-1} Fe·g $^{-1}$

t′ Time after maximum CO conversion, hours

TOS Time-on-stream, hours

U_g Superficial gas velocity based on inlet reactor conditions, cm s^{-1}

X_{CO} CO conversion

ϵ_g Gas hold up fraction in the reactor vessel, l l^{-1}

References

1. Davis, B. H., "Technology Development for Iron and Cobalt Fischer-Tropsch Catalysts," Quarterly Report #8, DE-FC26-98FT40308, July-Sept., 2000.
2. O'Dowd, W., J. Ruether, and S. Saxena, "Gas and Solids Behavior in a Baffled and Unbaffled Slurry Bubble Column", ***AIChE J.***, Vol.33, No. 12, pg. 1959-1970, December 1987.
3. Marretto, C. and R. Krishna, "Modeling of Bubble Column Slurry Reactor for Fischer-Tropsch Synthesis", ***Catalysis Today*** 52 (1999) 279-289.
4. Fogler, H., Elements of Chemical Reaction Engineering, 1st Edition, pgs. 273-278, Prentice-Hall, Englewood Cliffs, New Jersey 07632, 1986, ISBN 0-13-263476-7.

Table 1

Operating Conditions: SBCR and CSTR Comparison Experiments

	SBCR(LGX)	SBCR (JKN) (enhanced level control and filtration system)	CSTR(LX238)
Catalyst	4.4 Si/K	4.4 Si/K	4.4 Si/K
Initial Cat. loaded wt%	20	20	20
Catalyst. Activation:			
Gases	$CO+H_2$	CO	$CO+H_2$
H_2/CO	0.7	--	0.7
Gas space velocity (SL/hr-g Fe)	5.3	1.0	5.15
Temperature (^oC)	270	270	270
Pressure (atm.)	1	12	1
Synthesis Conditions:			
H_2/CO	0.7	0.7	0.7
Gas space velocity (SL/hr-g Fe)	5.3	5.2	5.15
Temperature (^oC)	270	270	270
Pressure (MPa)	1.21	1.21	1.21
Gas superficial velocity (cm/sec)	3	2.7	Stirred speed 750 RPM

Table 2

Slurry Bubble Column Measured Catalyst Concentration. Samples Taken During Shake Down Run (JKN-001)

Sample Location	wt% solids
Overhead Separation Vessel	10.93
Bottom-most reactor port.	13.11
Gas/liquid riser	10.42
Lower-middle reactor vessel port.	15.35

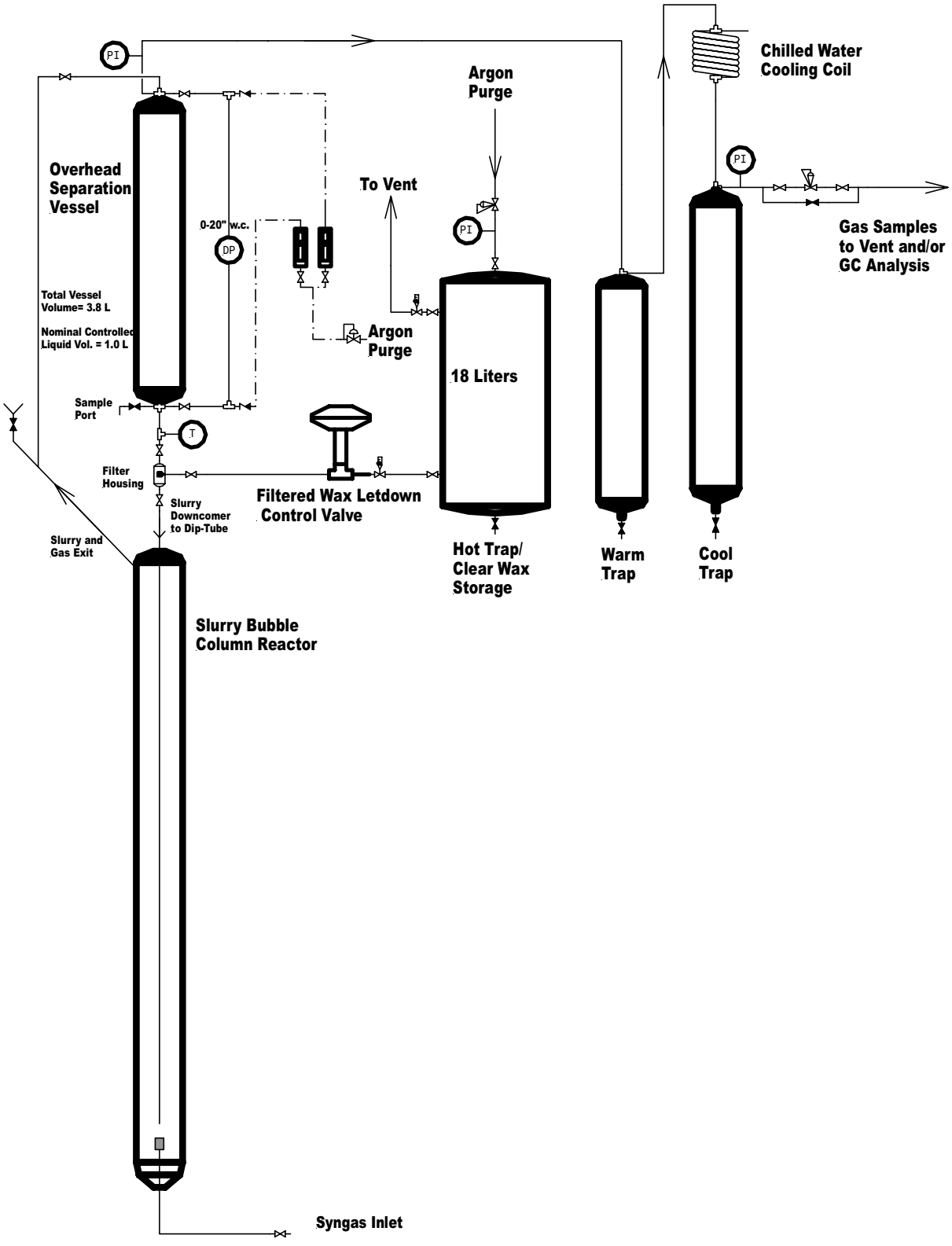

Figure 1. Schematic of the Enhanced Slurry Bubble Column Reactor Pilot Plant.

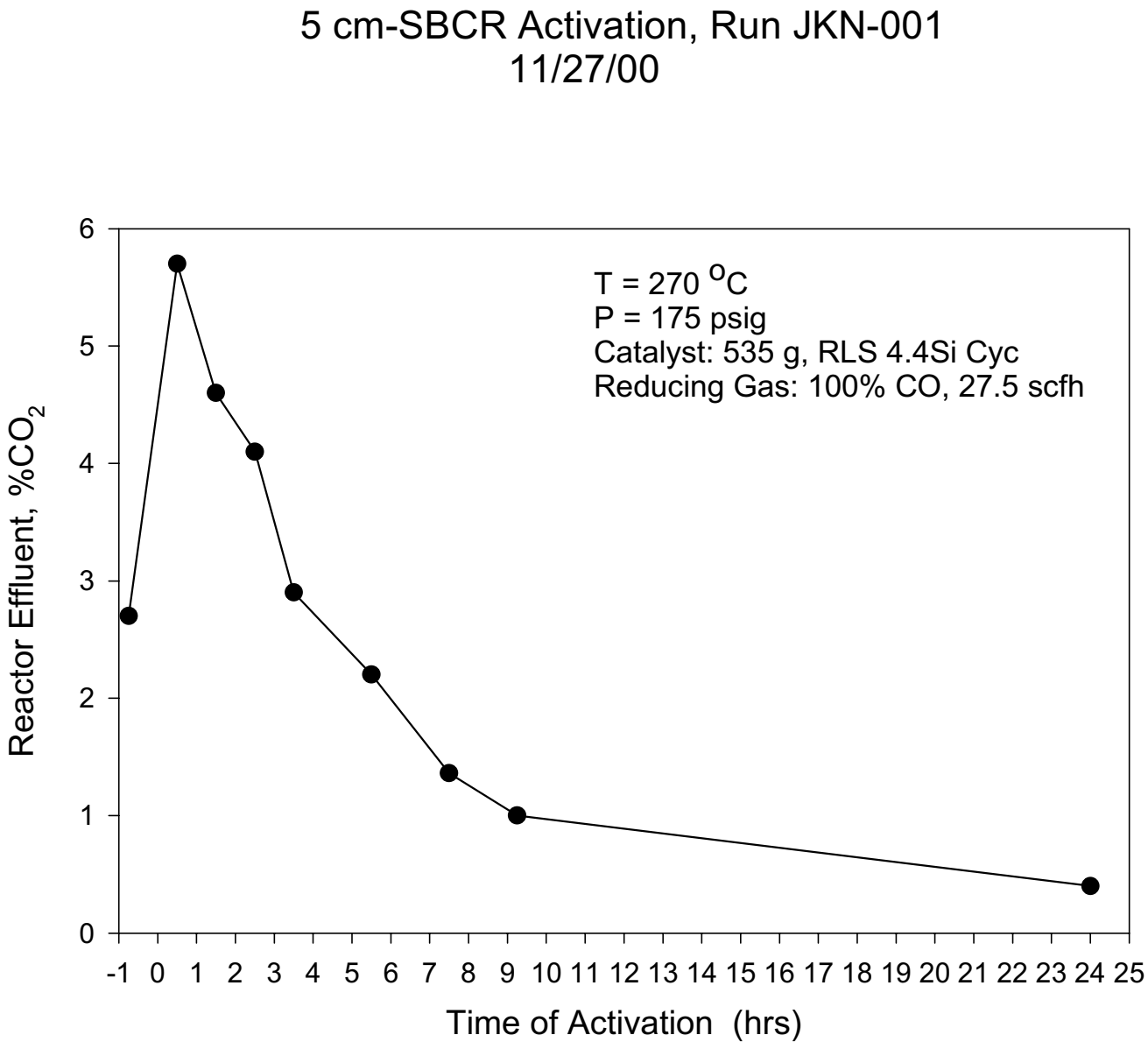

Figure 2. CO_2 exhaust profile during SBCR catalyst activation.

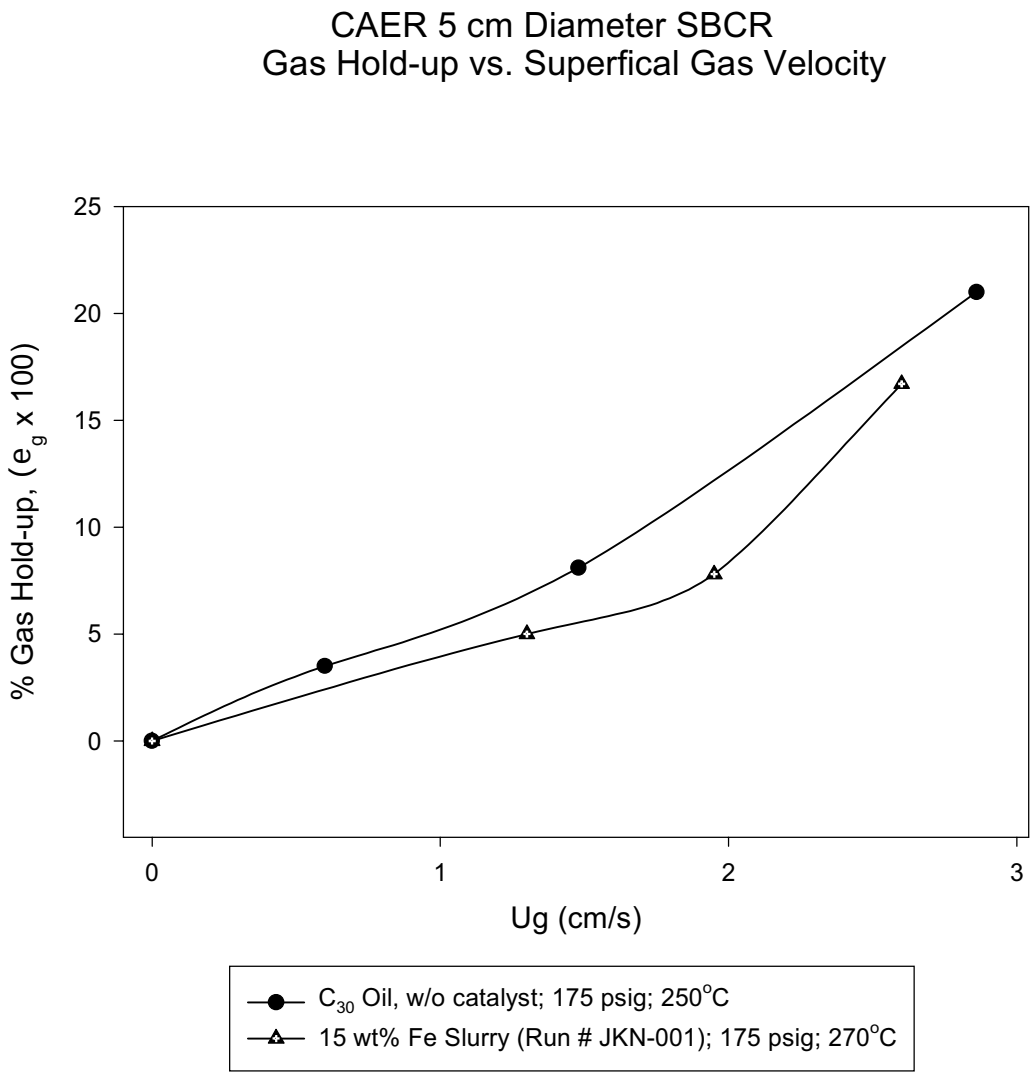

Figure 3. Measured gas hold up results vs. superficial velocity.

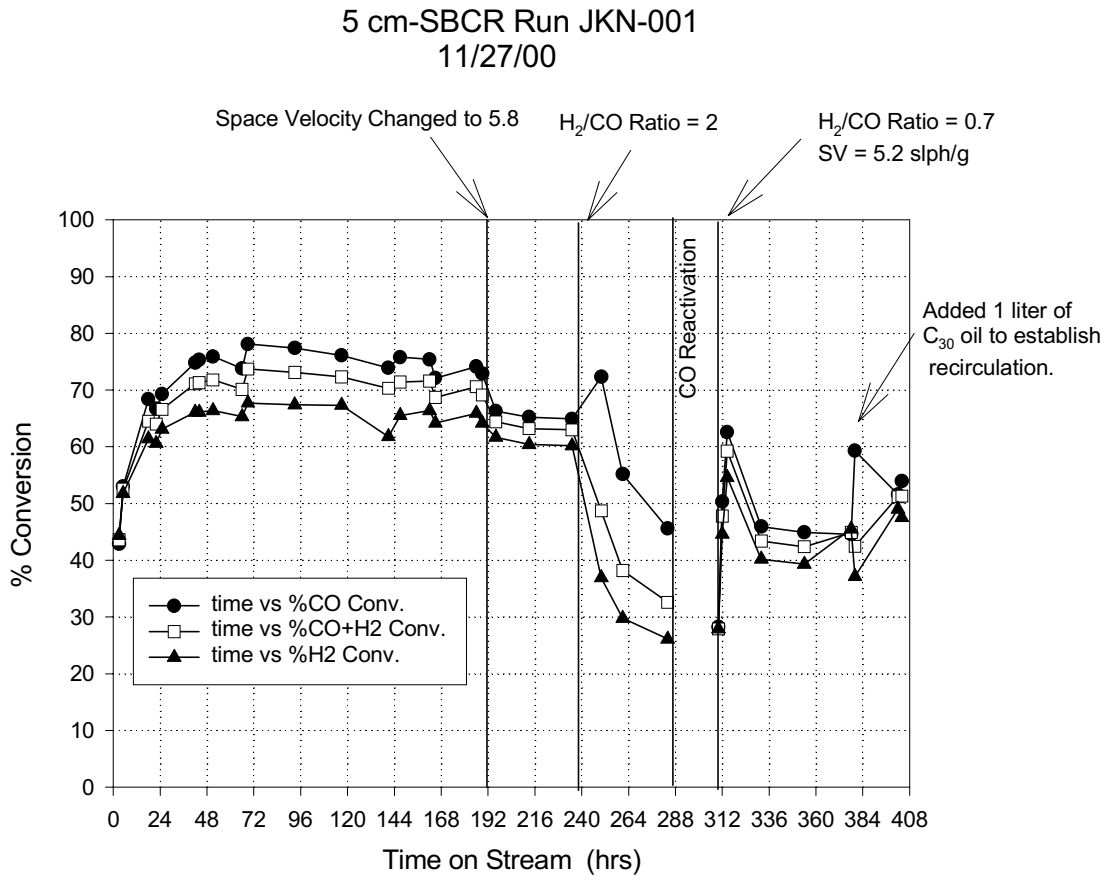

Figure 4. SBCR conversion vs. time on stream for the duration of the shake down run.

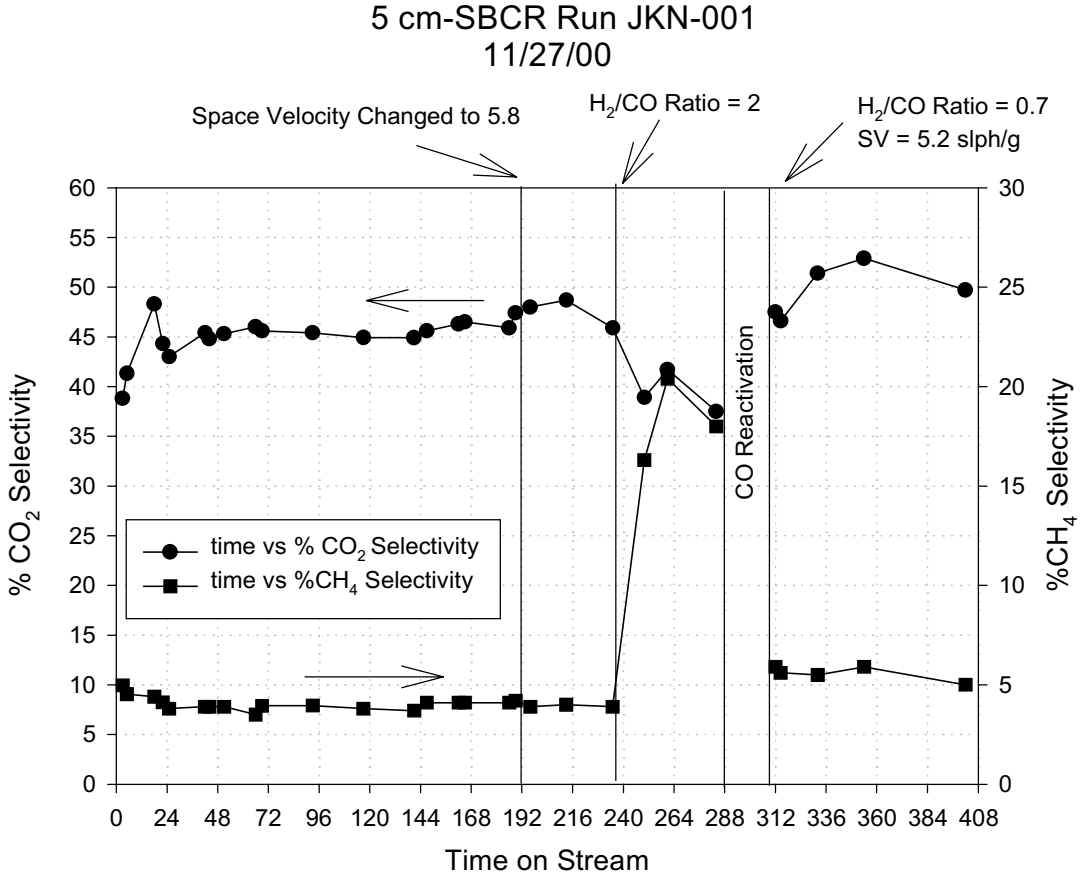

Starting Conditions:

T = 270 ^{O}C; P = 175 psig; H_2/CO Ratio = 0.7; SV = 5.2 slph/g Fe

Catalyst: RLS 4.4Si/K Cyc

Figure 5. SBCR CO_2 and CH_4 selectivity vs. time on stream for the duration of the shake down run.

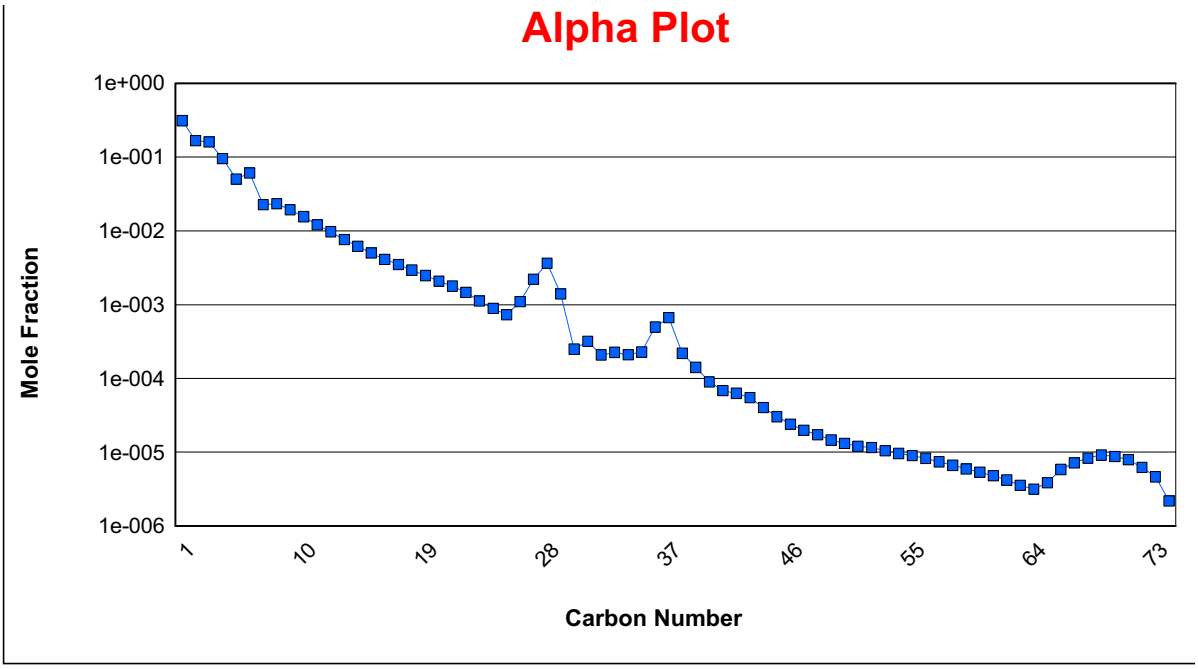

Figure 6. Alpha Plot Distribution for the Enhanced SBCR (run SBCR-JKN)

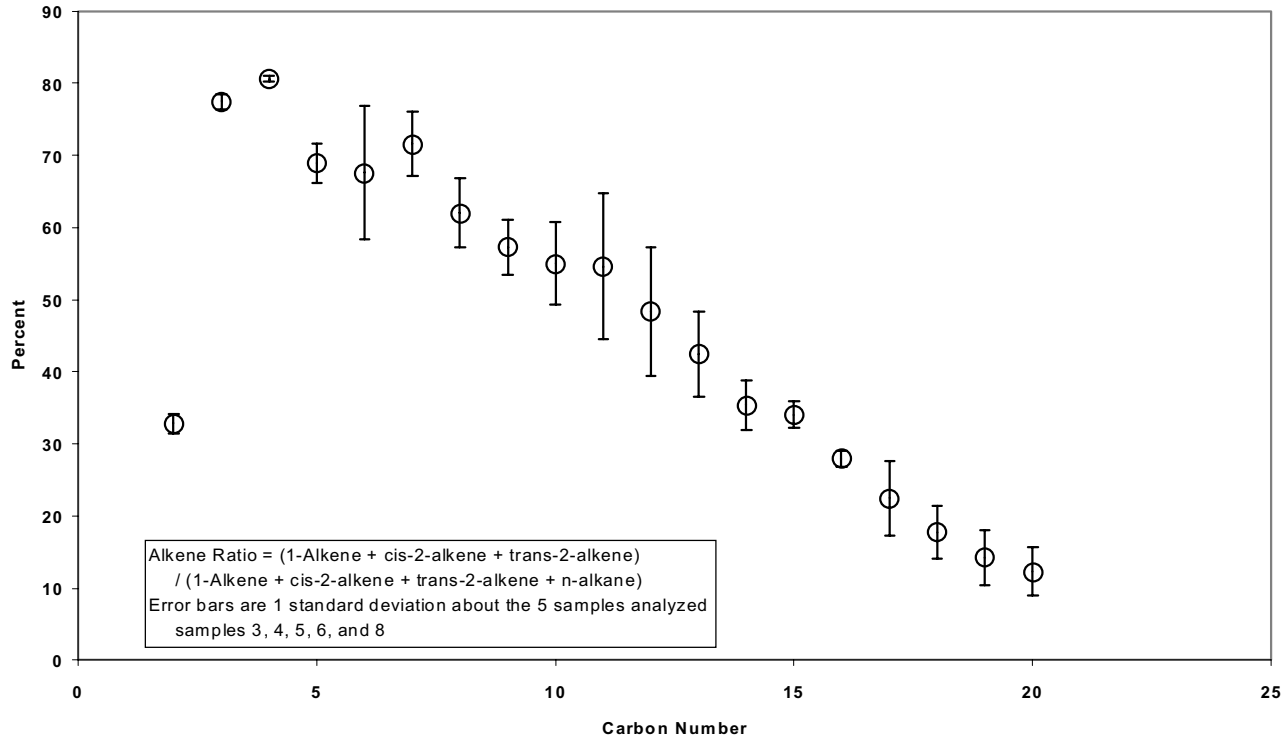

Figure 7. Alkene Ratios obtained with the enhanced SBCR (run# SBCR-JKN)Run Conditions: 270 oC, 175 psig, Catalyst RLS 4.4Si/K

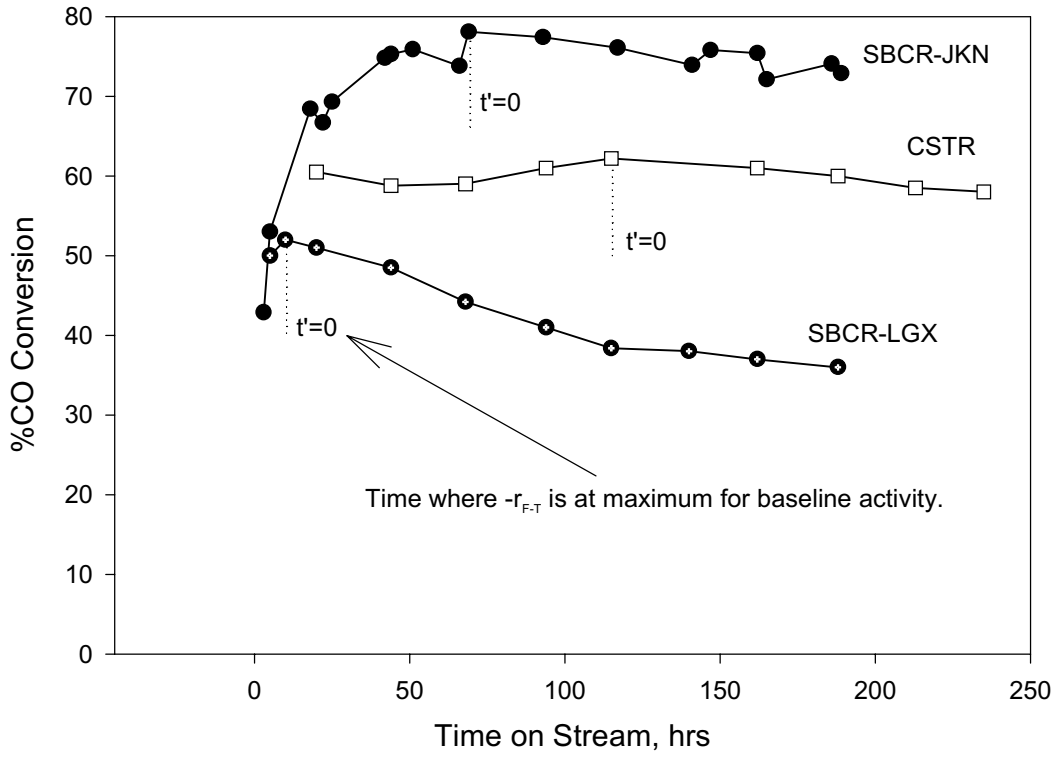

Figure 8. CO conversion comparison of SBCR and CSTR vs. time on stream.

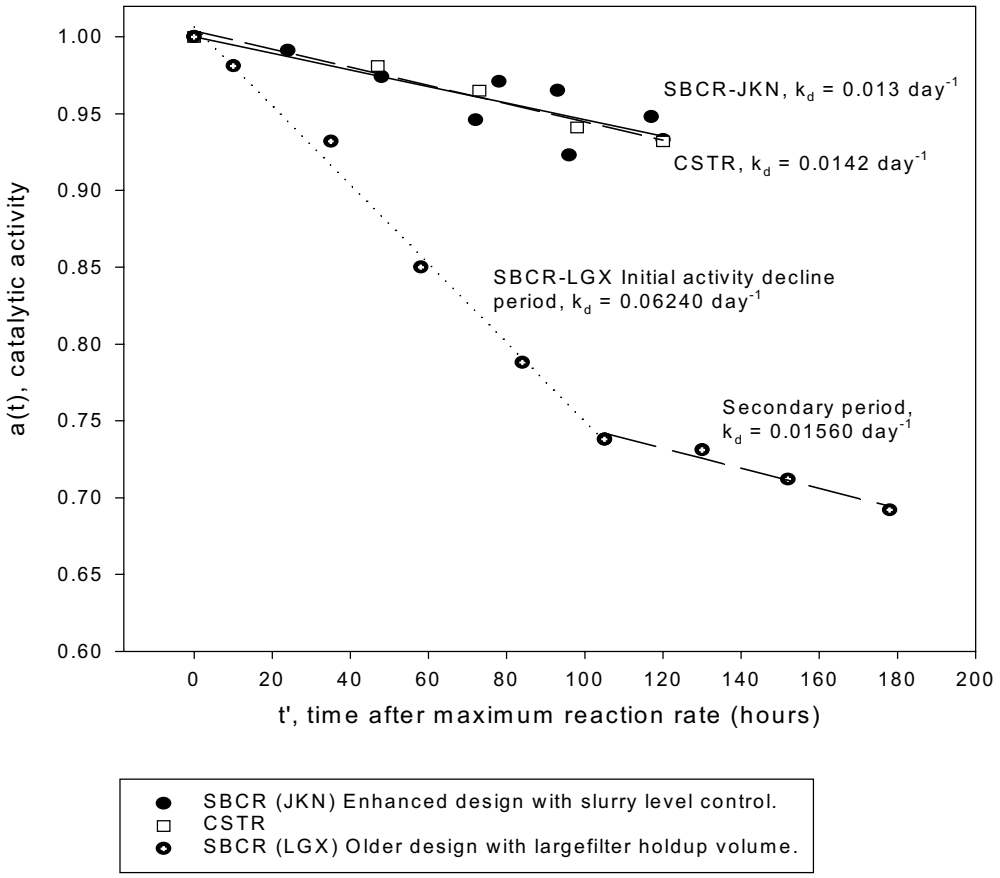

Figure 9. Catalyst deactivation comparison between SBCR and CSTR experiments.

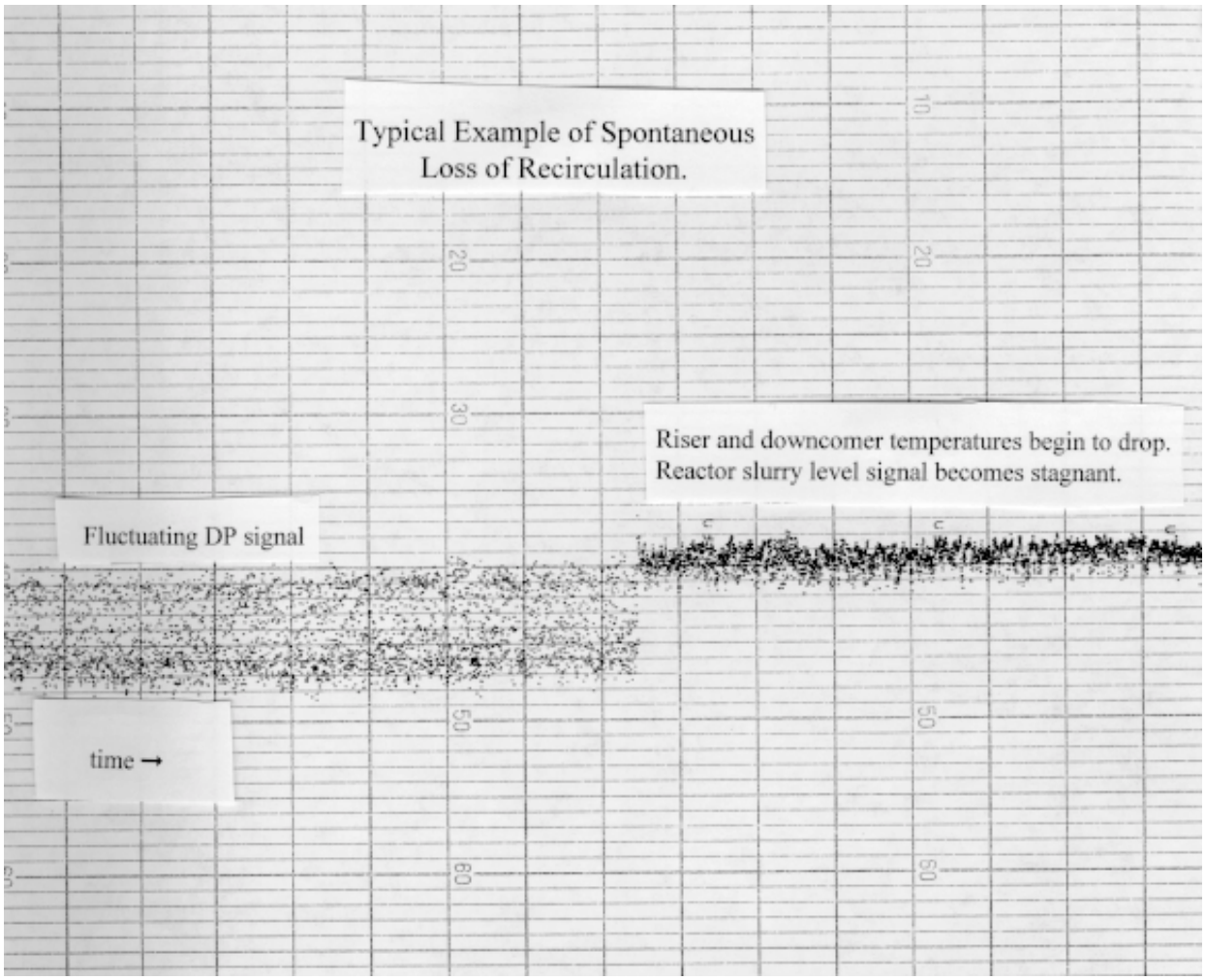

Figure 10. Overhead separation vessel level trace, with and without slurry recirculation.

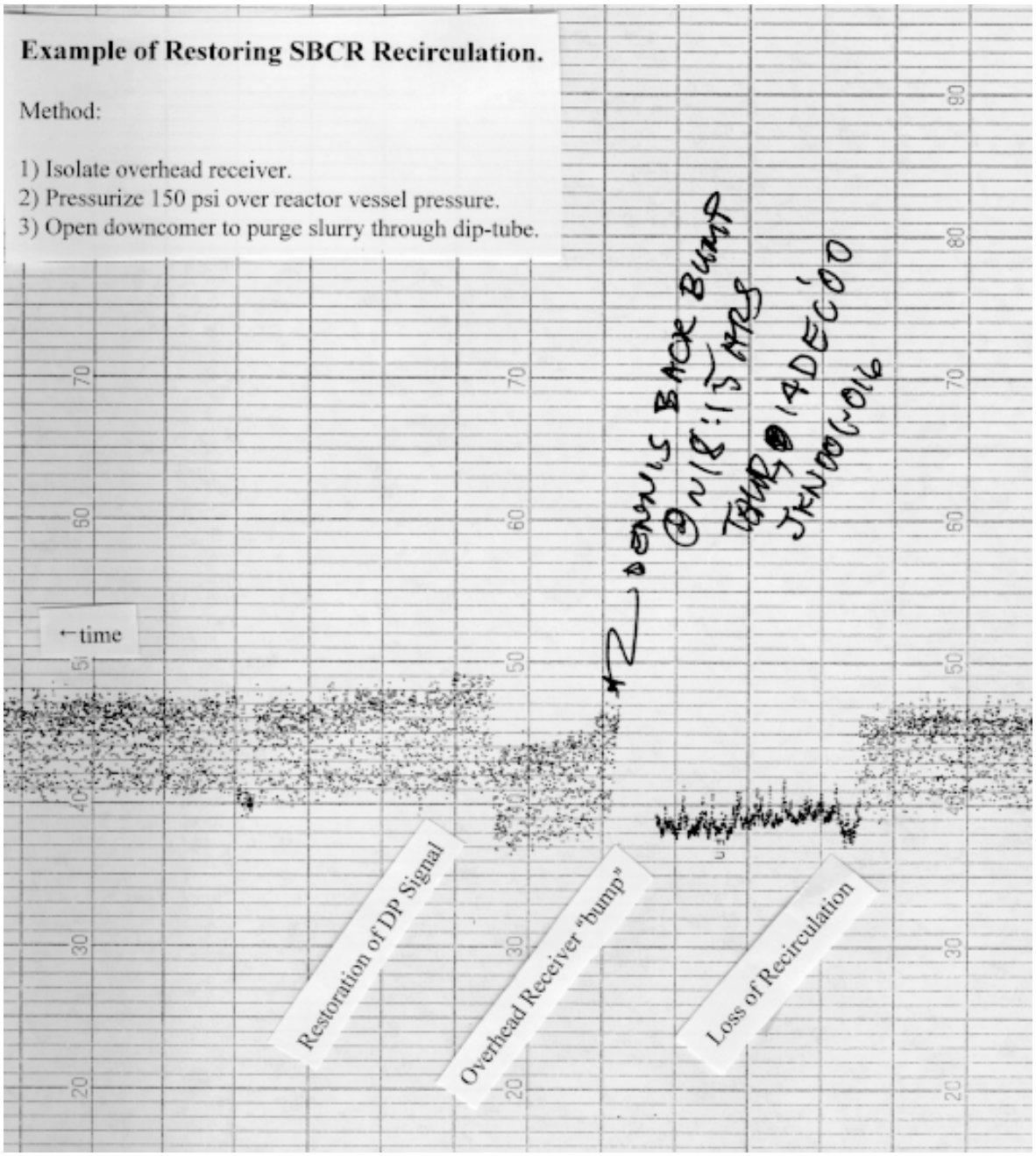

Figure 11. Overhead separation vessel level trace: reestablishment of slurry recirculation.